Relevance of thermal disorder in the electronic and spin ultrafast dynamics of iron in low perturbation regime

G. M. Pierantozzi*,[1,*] A. De Vita*,[1,2] R. Cucini,[1] A.M. Finardi,[1,2] T. Pincelli,[1,3] F. Sirotti,[4] J. Fujii,[1] C. Dri,[5] G. Brajnik,[5] R. Sergo,[5] G. Cautero,[5] G. Panaccione,[1,†] and G. Rossi[1,2]

[1] *Istituto Officina dei Materiali (IOM)-CNR, Laboratorio TASC, in Area Science Park, S.S.14, km 163.5, I-34149 Trieste, Italy*
[2] *Dipartimento di Fisica, Università degli Studi di Milano, Via Celoria 16, I-20133 Milano, Italy*
[3] *Fritz-Haber-Institut der Max-Planck-Gesellschaft, Faradayweg 4–6, Berlin 14195, Germany*
[4] *Physique de la Matiére Condensée, CNRS and École Polytechnique, Institut Polytechnique de Paris, Palaiseau, France*
[5] *Elettra Sincrotrone Trieste S.C.p.A, in Area Science Park, S.S.14 - km 163.5, I-34149 Trieste, Italy*

(Dated: January 9, 2024)

Understanding the ultrafast demagnetization of transition metals requires pump-probe experiments sensitive to the time evolution of the electronic, spin and lattice thermodynamic baths. By means of time-resolved photoelectron energy and spin polarization measurements in the low pump fluence regime on iron, we disentangle the different dynamics of hot electrons and demagnetization in the sub-ps and ps time range. We observe a broadening of the Fermi-Dirac distribution, following the excitation of non-thermal electrons at specific region of the iron valence band. The corresponding reduction of the spin polarization is remarkably delayed with respect to the dynamic of electronic temperature. The experimental results are corroborated with a microscopic 3-temperature model highlighting the role of thermal disorder in the quenching of the average spin magnetic moment, indicating Elliot-Yafet type spin-flip scattering as the main mediation mechanism, with a spin-flip probability of 0.1 and a rate of energy exchange between electrons and lattice of $2.5\,\mathrm{K\,fs^{-1}}$.

INTRODUCTION

Since the first observation of ultrafast demagnetization in a $3d$ ferromagnet following optical excitation [1], a variety of pump-probe techniques [2–9] have addressed this challenging aspect of band structure dynamics in solids. Up to date the observed phenomenology reveals i) a demagnetization within few hundreds of femtoseconds, ii) a partial recovery between approximately 200 fs to 1 ps, and iii) a relaxation to ground state in tens/hundreds of picoseconds. Recently, theoretical and experimental reports made increasingly clear that an explanation in the frame of a Stoner picture is insufficient [10, 11] and that temperature-dependent spin fluctuations play an important role [12, 13]. The statistical disorder in the spin degree of freedom can be included either by using a Weiss-Heisenberg model [14], or an *ad hoc* effective temperature-dependent exchange splitting [15, 16], or by introducing a band-mirroring mechanism [9, 17].

In this context, it is crucial to disentangle the relevance of spin thermal fluctuations from the contribution of electron spin redistribution in occupied and unoccupied bands [3, 9] and from the direct light-spin coupling [18]. An unmediated tool for such investigation is spin-resolved photoemission spectroscopy, only recently emerging in pump-probe experiments thanks to high-repetition rate lasers [8, 9, 19, 20]. In this Letter, we combine two different time-resolved (TR) photoemission techniques to investigate the ultrafast response of Fe(001)-p(1x1)O film, namely i) angular-resolved photoelectron spectroscopy (ARPES) to monitor changes in the electronic energy reservoir across the first Brillouin zone (fBZ) in an energy- and momentum-selective way [9, 19], and ii) Spin Polarization (SP) analysis of photoelectrons via Mott-scattering experiment to probe the evolution of the magnetic state [21]. We chose the Fe(001)-p(1x1)O surface as it is a well characterized ferromagnetic surfaces and robustness against contamination to ensure reproducible results in long experimental runs [22, 23]. The experiments were performed in the low perturbation regime, to avoid heating the electrons above the Curie temperature and to exclude temporarily collapse of the exchange splitting [24].

We clearly distinguish the thermalized electrons from those directly excited by the pump in a specific band, observing a thermalization time around 300 fs after the pump excitation. The dynamics of the spin polarization turns out to be markedly different with a delayed quenching. We explain the ensemble of the observations following a "microscopic" 3-Temperature Model (m-3TM) [25], which describes the heat transfer between electronic, spin and lattice baths accounting for microscopical scattering parameters, with a Weiss-Heisenberg picture for the spin system. As a result, we identify the ultrafast demagnetization in the low-fluence regime as mainly driven by thermal fluctuations. Fit results yield a spin-flip probability around 0.1 and an electron-lattice energy exchange rate of $2.5\,\mathrm{K\,fs^{-1}}$.

METHODS

The experiments were performed in the NFFA-Sprint laboratory at IOM-CNR, Trieste [26]. Measurements were conducted in Ultra-High Vacuum (UHV) at a pressure $< 3 \times 10^{-10}$ mbar. A 40 nm thick Fe(001) film was

grown *in situ* in a pressure $p < 2 \times 10^{-9}$ mbar epitaxially on a MgO(001) single crystal. The thickness was estimated by a quartz microbalance. A 30 min annealing at 800 K was followed by a 90 L O_2 exposure ($p = 1 \times 10^{-6}$ mbar at 450 K and a 30 s annealing at at 450 K to stabilize the p(1x1)O reconstruction [22]. The O overlayer is needed since it prevents contamination of the Fe surface for weeks in UHV. The sample is homogeneously magnetized along one in-plane easy axis, as proven by measuring vectorial SP across the sample: hereinafter we report only this in-plane direction. The SP values measured in two opposite azimuthal positions of the sample are used to cancel instrumental asymmetries; for time-resolved data, the values at negative delays are employed for such rescaling.

Linearly polarized pump ($h\nu = 1.55$ eV, 50 fs temporal width, s-polarized) and probe ($h\nu = 4.8$ eV, 160 fs, or $h\nu = 21.7$ eV, 110 fs, respectively for TR-SP or TR-ARPES, both s-polarized) pulses were used for time-resolved measurements. Pulsed radiation is generated by non-linear phenomena seeded by a pair of twin Light Conversion PHAROS lasers at 50 kHz, with 1.2 eV photon energy. To measure the SP at photothreshold, the fourth harmonic of one laser, produced by means of BBO crystals ($h\nu = 4.8$ eV, 160 fs temporal width, s-polarized), was used as probe beam. For angle-resolved photoemission (ARPES) spectra we employed a photon energy of 21.7 eV from a High Harmonic Generation (HHG) apparatus [26], pumped by the same laser (110 fs temporal width, s-polarized). The other PHAROS laser feeds an Optical Parametric Amplifier (OPA) delivering an energy-tunable pump beam (in this experiment fixed to 1.55 eV, s-polarized), 50 fs temporal width. The spot diameter, measured exploiting a YAG crystal at sample position, was 100 × 100 µm for the HHG beam, 550 × 300 µm for the 4.8 eV beam and 450 × 520 µm for the pump beam.

The SP of the total photoejected electrons (i.e. integrated in k and energy) was measured with a vectorial Mott polarimeter suitable for multi-hit detection [27]. The sample drain current was simultaneously acquired. TR-ARPES spectra were acquired by a Scienta SES 2002 hemispherical analyser. Additionally, static ARPES measurements were performed at the APE-LE beamline at Elettra synchrotron [23].

ULTRAFAST MAGNETIZATION QUENCHING

In total electron yield (TEY) mode, the contribution of secondary and inelastically scattered electrons can be minimized if photon energy slightly exceeds the sample work function (photothreshold) [28, 29], thus reducing spin-filtering effects [30–32] and preserving the initial-state SP. Threshold photoelectrons are integrated over 10-15 nm of material [33] so that the contribution from

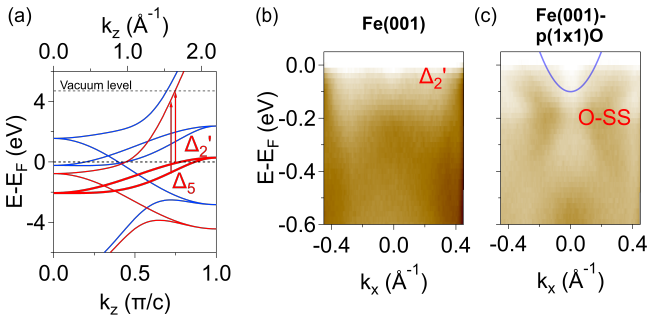

FIG. 1. (a) Density functional theory (DFT) calculations in the LDA approximation for Fe(001), showing the dispersion of the band structure at Γ as a function of k_z along $\Gamma - H$ direction. The available optical transitions to empty states close to the vacuum level for 4.8 eV are highlighted by arrows. (b-c) ARPES spectra along $\bar{\Gamma} - \bar{X}$ direction on clean Fe(001) and Fe(001)-p(1x1)O, measured with 25 eV, p-polarized synchrotron radiation. The parabola encloses the maximum E-k region accessed by 4.8 eV photons according to conservation rules, given a work function of 4.7 eV.

the surface oxygen is negligible. The possible initial states can be identified considering conservation laws in photoemission: with $h\nu = 4.8$ eV the signal arises from the neighborhood of E_F (< 0.1 eV) and from a limited range of $k_{\|}$ (< 0.2 Å^{-1}). A restriction in k_z is given by the available empty states: according to DFT calculations of bulk Fe bands at $\Gamma_{\|}$ along $\Gamma - H$ direction (Fig. 1a, in agreement with ref. [34]), there are only two possible direct transitions of 4.8 eV towards the vacuum level, with the (majority) $\Delta_{2\uparrow}$ and $\Delta_{5\uparrow}$ bands as initial states. Both transitions lie in the range of k_z expected for photoemission at threshold ($k_{z,PT} \approx 1.4 - 1.7$ Å^{-1} using inner potential values typically found in literature [34, 35]). The $\Delta_{2\uparrow}$ band can be identified in the small electron-like parabola ($k_F \approx 0.2$ Å^{-1}) observed on clean Fe(001) with $h\nu = 25$ eV (Fig. 1b); at such photon energy, the corresponding k_z verifies the same condition as $k_{z,PT}$ and allows to find $\Delta_{2\uparrow}$ close to E_F at $\Gamma_{\|}$. Such band is faintly visible also with the p(1x1)O reconstruction (Fig. 1c), although partially covered by the more intense O surface state (O-SS) with $k_F \approx 0.35$ Å^{-1}.

The SP measured with $h\nu = 4.8$ eV is 57(5) %, in excellent agreement with early work on bulk Fe at threshold [36]. A much lower value (20(3) %) is obtained well above threshold ($h\nu = 21.7$ eV), where the contribution of inelastic electrons dominates the TEY and averages over the full band SP. Since in both cases the SP has the same sign, the states probed by 4.8 eV must have majority character, as expected for electrons photoexcited from $\Delta_{2\uparrow}$ and $\Delta_{5\uparrow}$ bands. We can exclude any contribution to the SP from O-SS (of minority character [37]), as it lays outside the parabola in Fig. 1c determined by E-k conservation.

The effect of 1.55 eV pump pulses is presented in Fig.

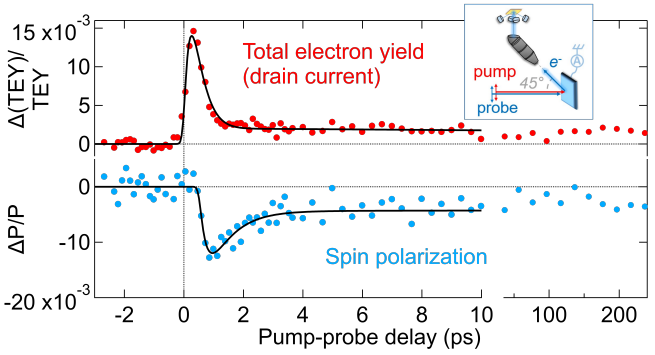

FIG. 2. Time-resolved relative variation of TEY (*top*) and SP (*bottom*) at 1.3 mJ/cm^2 pump fluence, using 4.8 eV probe and 1.55 eV pump. Inset: Experimental geometry.

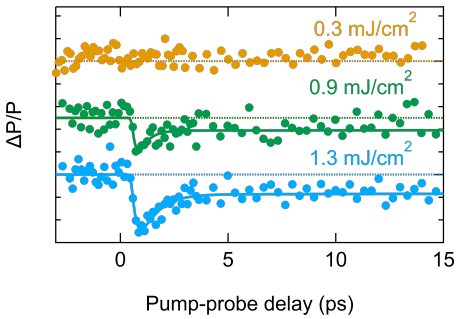

FIG. 3. Time-resolved relative variation of SP as a function of pump fluence.

2: we observe a transient decrease of the SP, partly recovered within few ps, still partially quenched at least up to 200 ps. The quenching depends on the fluence, for values not exceeding 0.3 mJ/cm^2 (Fig. 3). A phenomenological function [7, 8] with the addition of a long-living exponential [5] is used to fit the SP data (as well as the TEY curve in the *top* of Fig. 2):

$$\left\{\left[Q\left(1-e^{-\frac{t-t_0}{\tau_Q}}\right)\times\left(e^{-\frac{t-t_0}{\tau_R}}+Q_S e^{-\frac{t-t_0}{\tau_S}}\right)\right]\Theta(t,t_0)\right\} \quad (1)$$

where τ_Q is the quenching time constant and τ_R and τ_S describe respectively the fast and slow recovery (the latter fixed at 200 ps). The function is convoluted with a Gaussian accounting for the temporal resolution (fixed at 160 fs). For the investigated fluences (see Table I), τ_Q and τ_R are in good agreement with ultrafast demagnetization measurements at higher fluences, employing magneto-optical Kerr effect on *3d* transition metals [1, 24, 25, 38], and also specifically on Fe(001) on MgO(001) [5] or W(110) [7]. Our observation of a long-living demagnetized state is in contrast with the results of Tengdin et al. [24], who observe a slow-decaying tail only above the exchange splitting collapse threshold. We argue that the tail is linked to the heat diffusion, which takes hundreds of picoseconds to relax [5, 39].

Given the low photon energy, the peak and the following relaxation trend in the TEY curve in Fig. 2 can be attributed to the broadening of the electron distribution after the pump pulse. However, the TEY increase precedes the SP decrease and the TEY fast relaxation time (< 300 fs) is significantly smaller than τ_R. Given such differences with the electronic distribution evolution simultaneously measured, the observed SP behavior cannot be explained by the redistribution of spin-polarized carriers close to E_F, as proposed in previous experiments on Co [9] and Fe [20]. We also exclude superdiffusive spin currents [9] due to the insulating substrate and the long τ_Q. We thus propose that the observed SP reduction is an effect of the quenching of magnetic moment due to an increase of thermal disorder in the spin degree of freedom after the absorption of optical energy by the electrons. This picture is in agreement with recent theoretical findings on the parameters governing the ultrafast demagnetization [12].

TABLE I. Fit results of the SP dynamics.

Pulse energy (μJ)	Fluence (mJ/cm^2)	Q	τ_Q (fs)	τ_R (fs)
3.4	1.3	2.0%	290 ± 136	772 ± 138
2.3	0.9	1.3%	202 ± 82	436 ± 96

ULTRAFAST DYNAMICS OF ELECTRONS

We now accurately address the induced changes in the electronic distribution over the whole BZ, by means of ARPES with $h\nu = 21.7$ eV as probe (same 1.55 eV pump at 1.3 mJ/cm^2 at normal incidence) imaging the whole BZ by rotating the polar angle, with light polarization parallel to the rotation axis (Fig. 4a). Static ARPES measurements on p(1x1)O-Fe(001) are presented in Fig. 4b. Well-known O-induced states are located in the range from 4 eV to 6 eV binding energy (BE) [40, 41]. Close to E_F, we observe contributions from both bulk Fe and O overlayer (see Supplemental Material, Fig. S5).

TR-ARPES measurements have been carried out in three regions of the BZ (colored rectangles in Fig. 4b), displayed in panels c-e of Fig. 4, corresponding to incidence angles respectively of 15°, 34° and 65°, with effective fluence scaling accordingly. The sharp band in panel f is visible up to 0.4 eV above E_F in the pumped state at t_0 and almost disappearing after 300-500 fs. The integration over the selected k-region (displayed in Fig. 4f) shows that the fastest intensity rise occurs in the range 0.4-0.8 eV above E_F (*gold-green curves*), recovering to the equilibrium state within the pump pulse duration. The energy scale and the temporal behavior of such transient state - not observed in the other regions

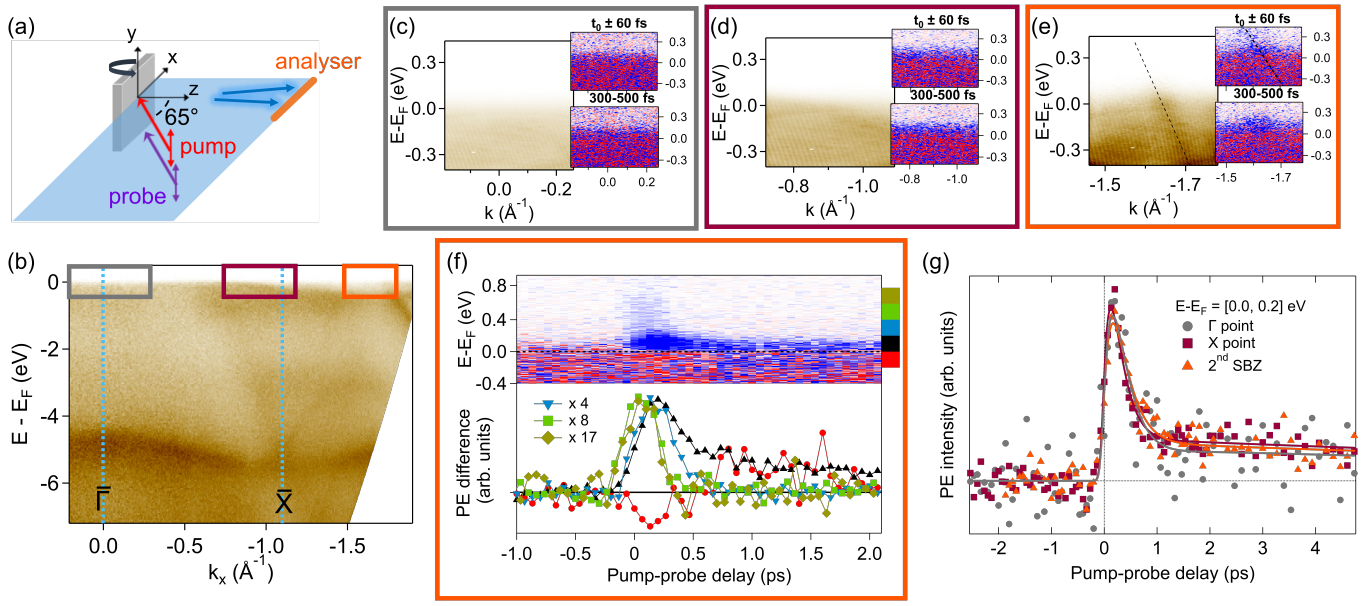

FIG. 4. (a) Cartoon representation of the TR-ARPES experimental geometry.(b) ARPES static measurement at 21.7 eV. (c-e) TR-ARPES with 1.55 eV pump and 21.7 eV probe, measured in the regions of panel (b) highlighted by the colored rectangles. *Main panel*: spectrum averaged over the temporal delays before t_0. *Insets*: in the *top* (*bottom*) one, difference between the spectrum at $t_0 \pm 60$ fs (300-500 fs) and the average before t_0 (blue positive, red negative). (f) k-integrated spectrum of panel (e) vs delay. *Top*: difference map after subtraction of the average before t_0 (blue positive, red negative). *Bottom*: delay cuts in the energy ranges indicated by the colored rods in the *top* panel, multiplied by arbitrary factors to compare their lineshapes. (g) Comparison of the behavior of thermal electrons in the three momentum regions highlighted in panel (b), with corresponding colors: the intensity difference integrated from 0 eV to 0.2 eV is rescaled to compensate different photoemission intensities due to pump fluence dependence on the incidence angle

.

of the BZ - cannot be explained by a broadening of the Fermi-Dirac distribution, hinting at a non-thermal nature [42, 43]. Some tens of femtoseconds later, a peak is reached also at lower energy, within 0.2 eV above E_F (*black curve*), with a concomitant decrease just below E_F (*red curve*), followed by a partial relaxation within 0.5 ps and by a long-living tail (see also Supplemental Material, Fig. S2). This behavior is compatible with a broadening of the Fermi step due to a temperature increase of the electron population, resulting from e-e scattering after the excitation of non-thermal electrons; the fast relaxation is due to thermalization with phonons [44]. The latter kind of trend is mirrored in the other regions of the BZ (Fig. 4g), confirming its thermal nature and the negligible dependence on the specific bands crossing Fermi level, as well as on the fluence (due to different incidence angles) within our low perturbation regime. We stress that such behavior of the electronic distribution around Fermi level is also independent of the coherent size of the p(1x1)O domains (see Supplemental Material, Fig. S6). Exploiting the fitting function in Eq. 1 (temporal width fixed to 110 fs), the thermalization time results 350(50) fs, in agreement with results on Fe/W(110) [19] and Co/Cu(001) [3], and the fast relaxation time 235(25) fs. Consistent results have been obtained with p-polarized probe and different pump energy (see Supplemental Material, respectively Fig. S3 and Fig. S4).

Since non-thermal electrons are observed only at $k_F = 1.65$ Å^{-1}, in the other regions we can describe the electron system using a time-dependent Fermi-Dirac distribution (FDD) at each pump-probe delay. The thermal process can be disentangled from the spectral function by means of the procedure described by Buhlmann et al. [20], which yields a function to be fitted with the FDD $f_{FD}(E;\mu,T_e) = (1+e^{-(E-\mu)/kT_e})^{-1}$ convoluted with an experimental Gaussian broadening, with chemical potential μ and electronic temperature T_e as free parameters. The former does not change within 1 meV, well below our energy resolution. The extracted T_e is displayed in Fig. 5 as a function of the delay for measurements at $\bar{X}$ (*top*, red dots), increasing up to 360 K (well below the Curie temperature) within few hundreds of fs, and then recovering to a value slightly above equilibrium. The small increase justifies *a posteriori* the assumption of a constant spectral function, *i.e.* no modifications in the band structure and especially in the exchange splitting, as expected for a maximum quenching of 1%.

DISCUSSION

To describe the heat transfer among different degrees of freedom we employ the m-3TM by Koopmans et al. [25], where the microscopic mechanism of phonon-mediated Elliot-Yafet spin-flip scattering is implemented in the temporal evolution of the spin system, treated with a Heisenberg Hamiltonian in the mean-field Weiss approximation. Here we suppose that the measured SP is related to the average magnetic moment m, on the basis of the discussion of Fig. 2. Additionally, following Carpene et al. [42], we add the non-thermal contributions $\partial U_{ee}/\partial t$ and $\partial U_{ep}/\partial t$ to the electronic and lattice differential equations, respectively; such terms describe the energy transfer from non-thermal electrons to thermal electrons and lattice, thus accounting for the slower thermalization compared to the laser pulse shape. This is modeled as a Gaussian profile, with temporal width fixed to 110 fs for T_e and 160 fs for m, and included into $\partial U_{ee}/\partial t$ and $\partial U_{ep}/\partial t$. No additional term is needed in the differential equation for m, since the spin dynamics results unaffected by the presence of non-thermal electrons, within our resolution. The equations read:

$$\gamma_e T_e \frac{dT_e}{dt} = -g_{ep}(T_e - T_p) + \frac{\partial U_{ee}}{\partial t}, \quad (2)$$

$$C_p \frac{dT_p}{dt} = -g_{ep}(T_p - T_e) - k(T_p - T_0) + \frac{\partial U_{ep}}{\partial t}, \quad (3)$$

$$\frac{dm}{dt} = Rm\frac{T_p}{T_C}\left(1 - m\coth\frac{mT_C}{T_e}\right). \quad (4)$$

The lattice specific heat C_p is assumed independent of temperature ($C_p = 3.527\,\mathrm{J/cm^3K}$) and the electronic specific heat as proportional to T_e through the factor $\gamma_e = 0.7\,\mathrm{mJ/cm^3K^2}$ [45]. The fit parameters are the electron-phonon coupling g_{ep} and the scaling factor R:

$$R = \frac{8a_{sf}g_{ep}k_B T_C^2 V_{at}}{(\mu_{at}/\mu_B)E_D^2}, \quad (5)$$

The fits of T_e and m curves according to the m-3TM have been performed independently, with consistent results (see Table II) and excellent agreement with data, as displayed in Fig. 5. By averaging the parameters in Table II and solving for a_{sf} in Eq. 5, we find $a_{sf} = 0.104(29)$, in line with values in literature for Ni and Co [25]. The resulting g_{ep} gives a good estimation of the rate for energy exchange between electrons and lattice, $g_{ep}/\gamma_e = 2.5\,\mathrm{K\,fs^{-1}}$, where the order of magnitude for most metals is around $1\,\mathrm{K\,fs^{-1}}$ [46].

The good agreement with a model in which the magnetic moment variation has intrinsically a thermal and collective origin supports the interpretation of SP at Fermi level in iron as reflecting the behavior of the average magnetic moment. The delayed dynamics of the spin degree of freedom observed here in low perturbation regime is well accounted by this model: the average magnetic moment starts changing only when the electrons have thermalized. The partial recovery of the magnetic moment within few picoseconds reflects the complete thermalization of the three different baths.

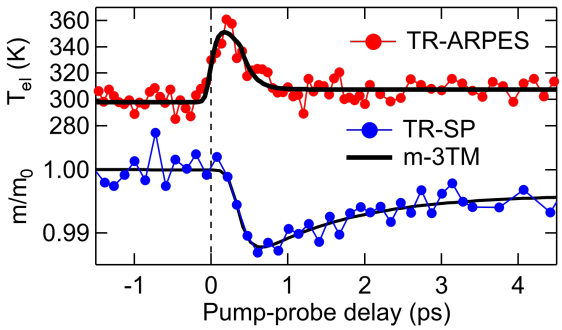

FIG. 5. Electronic temperature (*top*, from the TR-ARPES experiment) and relative magnetic moment (*bottom*, from the TR-SP experiment). Black lines are fits based on the m-3TM model. The temporal alignment has been retrieved using t_0 values obtained by the two independent fit procedures.

TABLE II. Fit results according to the m-3TM.

Fitted curves	g_{ep} 10^{18} J(sm^{3}K)$^{-1}$	R ps^{-1}
$T_e(t)$, X point	1.5(1)	2.5(5)
$m(t)$, 1.3 mJ/cm^2	1.8(2)	2.5(4)
$m(t)$, 0.9 mJ/cm^2	1.7(3)	2.5(7)

CONCLUSIONS

In conclusion, the electronic temperature and the magnetic moment at E_F after moderate optical excitation behave differently within 2-3 ps: the SP quenches only after the electron gas is fully heated and the thermalization with the lattice is activated, and then recovers with a larger time constant with respect to T_e. On the other hand, the trends of the long-living tail up to hundreds of picoseconds show a clear correspondence, signature of the thermalization of the three reservoirs. Our results demonstrate that in the low-fluence regime the transient spin variation is due to thermal fluctuations, driven by the increase of the electronic temperature upon pump excitation, once non-thermal electrons have transferred their excess energy to the whole electron bath.

ACKNOWLEDGEMENTS

This work has been performed in the framework of the Nanoscience Foundry and Fine Analysis (NFFA-MUR Italy Progetti Internazionali) facility.

Thanks are due to D. M. Janas, M. Cinchetti and C. H. Back for useful suggestions and discussion, and to A. Fondacaro and D. Krizmancic for technical support.

* G.M. Pierantozzi and A. De Vita contributed equally to this work.

* Corresponding author: pierantozzi@iom.cnr.it
† Corresponding author: panaccione@iom.cnr.it.

[1] E. Beaurepaire, J.-C. Merle, A. Daunois, and J.-Y. Bigot, Phys. Rev. Lett. **76**, 4250 (1996).
[2] J. Güdde, U. Conrad, V. Jähnke, J. Hohlfeld, and E. Matthias, Phys. Rev. B **59**, R6608 (1999).
[3] M. Cinchetti, M. Sánchez Albaneda, D. Hoffmann, T. Roth, J.-P. Wüstenberg, M. Krauß, O. Andreyev, H. C. Schneider, M. Bauer, and M. Aeschlimann, Phys. Rev. Lett. **97**, 177201 (2006).
[4] C. Stamm, T. Kachel, N. Pontius, R. Mitzner, T. Quast, K. Holldack, S. Khan, C. Lupulescu, E. F. Aziz, M. Wietstruk, H. A. Dürr, and W. Eberhardt, Nat. Mat. **6**, 740 (2007).
[5] E. Carpene, E. Mancini, C. Dallera, M. Brenna, E. Puppin, and S. De Silvestri, Phys. Rev. B **78**, 174422 (2008).
[6] C. La-O-Vorakiat, M. Siemens, M. M. Murnane, H. C. Kapteyn, S. Mathias, M. Aeschlimann, P. Grychtol, R. Adam, C. M. Schneider, J. M. Shaw, H. Nembach, and T. J. Silva, Phys. Rev. Lett. **103**, 257402 (2009).
[7] A. Weber, F. Pressacco, S. Günther, E. Mancini, P. M. Oppeneer, and C. H. Back, Phys. Rev. B **84**, 132412 (2011).
[8] A. Fognini, T. U. Michlmayr, G. Salvatella, C. Wetli, U. Ramsperger, T. Bähler, F. Sorgenfrei, M. Beye, A. Eschenlohr, N. Pontius, C. Stamm, F. Hieke, M. Dell'Angela, S. d. Jong, R. Kukreja, N. Gerasimova, V. Rybnikov, A. Al-Shemmary, H. Redlin, J. Raabe, A. Föhlisch, H. A. Dürr, W. Wurth, D. Pescia, A. Vaterlaus, and Y. Acremann, Applied Physics Letters **104**, 032402 (2014).
[9] S. Eich, M. Plötzing, M. Rollinger, S. Emmerich, R. Adam, C. Chen, H. C. Kapteyn, M. M. Murnane, L. Plucinski, D. Steil, B. Stadtmüller, M. Cinchetti, M. Aeschlimann, C. M. Schneider, and S. Mathias, Science Advances **3**, e1602094 (2017).
[10] E. Carpene, H. Hedayat, F. Boschini, and C. Dallera, Phys. Rev. B **91**, 174414 (2015).
[11] E. Turgut, D. Zusin, D. Legut, K. Carva, R. Knut, J. M. Shaw, C. Chen, Z. Tao, H. T. Nembach, T. J. Silva, S. Mathias, M. Aeschlimann, P. M. Oppeneer, H. C. Kapteyn, M. M. Murnane, and P. Grychtol, Phys. Rev. B **94**, 220408(R) (2016).
[12] Z. Chen and L.-W. Wang, Science Advances **5**, eaau8000 (2019).
[13] J. Minár, S. Mankovsky, J. Braun, and H. Ebert, Phys. Rev. B **102**, 035107 (2020).
[14] A. J. Schellekens and B. Koopmans, Phys. Rev. Lett. **110**, 217204 (2013).
[15] B. Y. Mueller, A. Baral, S. Vollmar, M. Cinchetti, M. Aeschlimann, H. C. Schneider, and B. Rethfeld, Phys. Rev. Lett. **111**, 167204 (2013).
[16] A. L. Chekhov, Y. Behovits, J. J. F. Heitz, C. Denker, D. A. Reiss, M. Wolf, M. Weinelt, P. W. Brouwer, M. Münzenberg, and T. Kampfrath, Phys. Rev. X **11**, 041055 (2021).
[17] B. Andres and M. Weinelt, Journal of Magnetism and Magnetic Materials **501**, 166475 (2020).
[18] J.-Y. Bigot, M. Vomir, and E. Beaurepaire, Nature Phys. **5**, 515 (2009).
[19] R. Gort, K. Bühlmann, S. Däster, G. Salvatella, N. Hartmann, Y. Zemp, S. Holenstein, C. Stieger, A. Fognini, T. U. Michlmayr, T. Bähler, A. Vaterlaus, and Y. Acremann, Phys. Rev. Lett. **121**, 087206 (2018).
[20] K. Bühlmann, G. Saerens, A. Vaterlaus, and Y. Acremann, Structural Dynamics **7**, 065101 (2020).
[21] T. J. Gay and F. B. Dunning, Review of Scientific Instruments **63**, 1635 (1992).
[22] R. Bertacco and F. Ciccacci, Phys. Rev. B **59**, 4207 (1999).
[23] C. Bigi, P. K. Das, D. Benedetti, F. Salvador, D. Krizmancic, R. Sergo, A. Martin, G. Panaccione, G. Rossi, J. Fujii, and I. Vobornik, Journal of Synchrotron Radiation **24**, 750 (2017).
[24] P. Tengdin, W. You, C. Chen, X. Shi, D. Zusin, Y. Zhang, C. Gentry, A. Blonsky, M. Keller, P. M. Oppeneer, H. C. Kapteyn, Z. Tao, and M. M. Murnane, Science Advances **4**, eaap9744 (2018).
[25] B. Koopmans, G. Malinowski, F. Dalla Longa, D. Steiauf, M. Fähnle, T. Roth, M. Cinchetti, and M. Aeschlimann, Nature Mater. **9**, 259 (2010).
[26] R. Cucini, T. Pincelli, G. Panaccione, D. Kopic, F. Frassetto, P. Miotti, G. M. Pierantozzi, S. Peli, A. Fondacaro, A. De Luisa, A. De Vita, P. Carrara, D. Krizmancic, D. T. Payne, F. Salvador, A. Sterzi, L. Poletto, F. Parmigiani, G. Rossi, and F. Cilento, Structural Dynamics **7**, 014303 (2020).
[27] T. Pincelli, V. N. Petrov, G. Brajnik, R. Ciprian, V. Lollobrigida, P. Torelli, D. Krizmancic, F. Salvador, A. De Luisa, R. Sergo, A. Gubertini, G. Cautero, S. Carrato, G. Rossi, and G. Panaccione, Review of Scientific Instruments **87**, 035111 (2016).
[28] H. E. Farnsworth, Phys. Rev. **27**, 413 (1926).
[29] A. Bellissimo, G. M. Pierantozzi, A. Ruocco, G. Stefani, O. Y. Ridzel, V. Astašauskas, W. S. Werner, and M. Taborelli, Journal of Electron Spectroscopy and Related Phenomena **241**, 146883 (2020).
[30] E. Kisker, W. Gudat, and K. Schröder, Solid State Communications **44**, 591 (1982).
[31] H. Hopster, R. Raue, E. Kisker, G. Güntherodt, and M. Campagna, Phys. Rev. Lett. **50**, 70 (1983).
[32] M. Aeschlimann, M. Bauer, S. Pawlik, W. Weber, R. Burgermeister, D. Oberli, and H. C. Siegmann, Phys. Rev. Lett. **79**, 5158 (1997).
[33] G. K. L. Marx, P.-O. Jubert, A. Bischof, and R. Allenspach, Applied Physics Letters **83**, 2925 (2003).
[34] E. Młyńczak, M. Eschbach, S. Borek, J. Minár, J. Braun, I. Aguilera, G. Bihlmayer, S. Döring, M. Gehlmann, P. Gospodarič, S. Suga, L. Plucinski, S. Blügel, H. Ebert, and C. M. Schneider, Phys. Rev. X **6**, 041048 (2016).
[35] E. Młyńczak, I. Aguilera, P. Gospodarič, T. Heider, M. Jugovac, G. Zamborlini, C. Tusche, S. Suga, V. Feyer, S. Blügel, L. Plucinski, and C. M. Schneider, Phys. Rev. B **103**, 035134 (2021).
[36] W. Eib and B. Reihl, Phys. Rev. Lett. **40**, 1674 (1978).
[37] A. M. Finardi, Bachelor's degree thesis: All-resolved photoemission spectroscopy of Fe(100) and passivated Fe-p(1x1)O surfaces (2020).

[38] A. J. Schellekens, W. Verhoeven, T. N. Vader, and B. Koopmans, Applied Physics Letters **102**, 252408 (2013).
[39] T. Pincelli, R. Cucini, A. Verna, F. Borgatti, M. Oura, K. Tamasaku, H. Osawa, T.-L. Lee, C. Schlueter, S. Günther, C. H. Back, M. Dell'Angela, R. Ciprian, P. Orgiani, A. Petrov, F. Sirotti, V. A. Dediu, I. Bergenti, P. Graziosi, F. Miletto Granozio, Y. Tanaka, M. Taguchi, H. Daimon, J. Fujii, G. Rossi, and G. Panaccione, Phys. Rev. B **100**, 045118 (2019).
[40] G. Panzner, D. R. Mueller, and T. N. Rhodin, Phys. Rev. B **32**, 3472 (1985).
[41] D. M. Janas, A. Droghetti, S. Ponzoni, I. Cojocariu, M. Jugovac, V. Feyer, M. M. Radonjić, I. Rungger, L. Chioncel, G. Zamborlini, and M. Cinchetti, Advanced Materials **35**, 2205698 (2023).
[42] E. Carpene, Phys. Rev. B **74**, 024301 (2006).
[43] M. Uehlein, S. T. Weber, and B. Rethfeld, Nanomaterials **12**, 10.3390/nano12101655 (2022).
[44] N. Del Fatti, C. Voisin, M. Achermann, S. Tzortzakis, D. Christofilos, and F. Vallée, Phys. Rev. B **61**, 16956 (2000).
[45] L. Kaufman, E. Clougherty, and R. Weiss, Acta Metallurgica **11**, 323 (1963).
[46] G. Ferrini, F. Banfi, C. Giannetti, and F. Parmigiani, Nuclear Instruments and Methods in Physics Research Section A: Accelerators, Spectrometers, Detectors and Associated Equipment **601**, 123 (2009).